JOURNAL OF Applied Polymer SCIENCE

Effects of Periodic and Non-Periodic Chaotic Mixing on Morphology Development of Immiscible Polymer Blends

Jia-Jun Wang, Yi-Wei Yang, Xue-Ping Gu, Lian-Fang Feng
State Key Laboratory of Chemical Engineering, Department of Chemical and Biological Engineering, Zhejiang University, Hangzhou 310027, People's Republic of China
Correspondence to: L.-F. Feng (E-mail: fenglf@zju.edu.cn)

ABSTRACT: The effects of periodic and non-periodic chaotic mixing on the morphology development in the blending of polypropylene as dispersed phase and polyamide 6 as continuous phase in a 2D batch chaotic mixer were investigated with experimental and computational fluid dynamic (CFD) methods. The rotor motions were delivered in steady, periodic (sine waveform and square waveform), and non-periodic (recursive protocol (RP) and restricted random sequence (RRS)) manners. The mixing efficiency was evaluated with flow number, Poincare map, morphology, droplet size and its distribution. Compared with the sine waveform, RP waveform could eliminate the island structures which existed in the flow domains and its corresponding spatial stretching distribution was more uniform. The recursively generated flow using RP lead to higher mixing efficiency and smaller droplet size with narrow distribution. However, the performance of RRS was ordinary even worse due to its random sequence.© 2012 Wiley Periodicals, Inc. J. Appl. Polym. Sci. 000: 000–000, 2012

KEYWORDS: chaotic mixing; blends; morphology; processing; computational fluid dynamic

Received 1 September 2011; accepted 6 July 2012; published online
DOI: 10.1002/app.38309

INTRODUCTION

Microstructure of immiscible polymer blends strongly influences the material performance. Twin-screw extruders and internal mixers are used widely as traditional polymer blending equipments and can provide strong shear to break the dispersed phase into micro-droplets quickly and form sea-island structure eventually. However, blends with sea-island structure are not suitable for some special applications, like conductive polymers, barrier materials, and so on. In addition, the intensive shear may break down chemical bonds of polymers, degrading the performance of polymer materials.

Morphology development in immiscible polymers occurs through transformation of dispersed phase into lamellas, fibrils, and finally to droplets.[1–5] The lamellar structures, which are formed in the early stages of mixing, undergo interfacial instabilities beyond a critical lamella thickness, and eventually transform into fibrillar structures.[6] The fibrils will undergo the capillary instability and break up into droplets. The newly formed droplets will break up again if their sizes are larger than the equilibrium diameter, or they will tend to coalesce, finally a pseudo-equilibrium state is reached.[7] In twin-screw extruders and internal mixers, it is difficult to achieve the lamellar and fibrillar structures due to the fast transformation of morphologies.

The striation thickness of lamellas decreases linearly with time in traditional mixing flows, such as those encountered in single and twin-screw extruders,[8–10] but exponentially in chaotic mixing flows,[11–13] which are generated by time-periodic motion of boundaries[14–19] or spatially periodic variation of flow channel geometry.[6,11,20] In chaotic mixing, the dispersed phase initially produces self-similar lamellar structures,[21] by stretching and folding both minor and major components of blends. Therefore, very thin lamellae and high aspect ratio fibrils are easily formed, leading to small droplets with narrow distribution.

Fundamental studies on the mechanism of chaotic mixing have been conducted in nonlinear dynamic theory from a theoretical point of view since the pioneering work of Aref[14] and Ottino.[15] Zumbrunnen and coworkers[22–26] were the first to study the blending of polymers by chaotic mixing. They used two designs of batch chaotic mixing devices such as a journal bearing[24] and an eccentric disk chaotic mixer (EDCM)[23] to investigate the morphology development in polymer blends at various compositions. In addition, a continuous chaotic mixing device[26] was developed to produce blends of various forms (film, sheet, etc.) with a variety of morphologies in continuous lengths. The process, called as smart blending,[25,27] can offer unprecedented control of internal structure development. Jana and coworkers,[7,28,29] designed a 2D batch chaotic mixer, and investigated the effects

of chaotic mixer geometry, operating parameter, mixing waveforms, viscosity ratio, and composition of polymer blends on the development of morphology. They proposed a sine waveform, which could eliminate the weak stretching domain existing in the flow produced by square waveform and gave polymer blends more uniform stretching to produce fibrils with higher aspect ratio up to 10,000 and droplets with smaller size.

In a time-periodic chaotic flow, the mixed zone includes chaotic region and regular region (island). A regular region is one in which each fluid particle returns, at the end of each period, to some location on a fixed orbit. According to Kolmogorov–Arnold–Moser (KAM) theorem in the dynamic system, a fluid in the unmixed island cannot mix with their surroundings. Thus, the time-periodic chaotic mixing gives uneven distribution of mixing process with high mixing efficiency in chaotic zone and poor mixing in island.

For enhancing the mixing, Franjione et al.[30] proposed a recursive protocol (RP) to effectively eliminate the islands through destructing the symmetry of periodic mixing. The recursively generated flow history is neither periodic nor random, but is self-similar. Mixing process for RP is efficient over the entire flow domain, and is better than the corresponding periodic protocol. Liu et al.[31] used stretching field to quantitatively analyze the effect of non-periodic flow with numerical simulation, and pointed out that non-periodic flow gives more homogeneous stretching distribution. The non-periodic mixing protocol was used by Zumbrunnen and co-workers[24,32] to promote more uniform stretching at the late stage of mixing. Fan and Lu[33] investigated the periodic and non-periodic chaotic flows in an eccentric cylinder through flow visualization experiments and numerical simulations. They gave a random restriction series (RRS) which also can reveal perfect mixing. Until now, there is no systematically relevant report on the application of non-periodic chaotic mixing in polymer blends.

In this article, the effects of periodic and non-periodic mixing on morphology development between polypropylene (PP) as dispersed phase and polyamide 6 (PA6) as continuous phase are presented. A 2D chaotic mixer, which was similar to that designed by Sau and Jana,[28] was used along with a Brabender torque rheometer as a traditional mixer for comparison. A square waveform and a sine waveform were used for periodic mixing, while a RP and a RRS were designed for non-periodic chaotic mixing. The computational fluid dynamic (CFD) method was used to investigate the chaotic mixing flow. Three issues were considered in this study: (a) the mixing process with temporal sequence through the flow number distribution and Poincare map; (b) the features of morphology development of polymer blends using periodic and non-periodic chaotic mixing; (c) the comparison of droplet sizes and its distributions using periodic, non-periodic chaotic mixing, and traditional mixing.

EXPERIMENTAL

Materials

PA6 (1013B, melt flow index of 40.4, UBE Nylon, Yamaguchi-ken, Japan) was used as the continuous phase, while PP (F401, melt flow index of 2.6, Sinopec, Yizheng, China) as the dispersed phase. The blend contained 90 wt % of PA6. The crystalline melting temperatures of PA6 and PP were 224 and 167°C, while their crystallization temperatures were 179 and 113°C, respectively, based on measurements by differential scanning calorimetry (DSC7, Perkin-Elmer Inc, Waltham, Massachusetts). Figure 1 shows the steady shear viscosities of the polymers and were determined by an HAAKE cone and plate rheometer (RS 6000, Thermo Fisher Scientific, Schwerte, Germany) at 245°C. The ratio of the zero shear viscosity of PP to PA6 was found to be around 4.

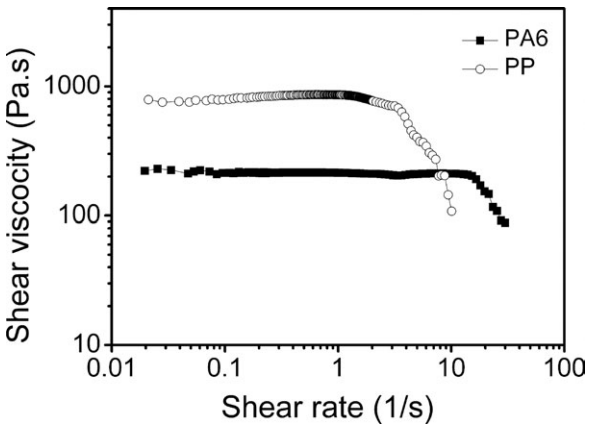

Figure 1. Shear viscosity of PP and PA6 at 245°C.

Chaotic Mixing Device

Polymer blends were mixed in a batch chaotic mixer [Figure 2(a)] and a Brabender torque rheometer (Plasti-Corder Lab-Station, Brabender GmbH & Co). The batch chaotic mixer was similar to that of Sau and Jana.[28] The mixer consisted of three parts, i.e., mixing chamber, stirring device, and heating device. The cross-sectional shape of the mixing chamber [Figure 2(b)] was similar to that of twin-screw extruder. Two circular rotors A (Left) and B (Right) with the diameter of 0.0254 m were used to maintain a shear gap (d, between the stationary walls and the rotors) of 0.0127 m. The mixing chamber with a depth of 0.0178 m was deeper than that of Sau and Jana's device, and approximately 36 g of materials could be produced at a time. The stirring device was driven by two step motors, which were controlled through two-step motor drivers and a motion controlling card. A 1000 W band heater surrounding the mixing chamber was used for heating. In addition, the Brabender torque rheometer, with a mixing chamber of volume 50 cm^3 and two roller blades with the same speed and contrary direction, was used as a traditional mixer to mix the materials for comparison.

Waveforms of Rotor Motion

For achieving periodic chaotic mixing, the speeds of rotors A and B followed a sine waveform proposed by Jana and Sau,[7] as shown in eq. (1) and a square waveform as expressed in eq. (2).

$$\Omega_A = \frac{\Omega}{2}\left(1 - \cos\frac{2\pi t}{T}\right), \quad \Omega_B = \frac{\Omega}{2}\left(1 + \cos\frac{2\pi t}{T}\right), \quad 0 \le t \le T \tag{1}$$

$$\begin{aligned} &\Omega_A = \Omega, \ \Omega_B = 00 \le t \le \frac{T}{2} \\ &\Omega_A = 0, \ \Omega_B = \Omega\frac{T}{2} \le t \le T \end{aligned} \tag{2}$$

where Ω_A and Ω_B are the angular speeds for rotors A and B in the same direction, respectively. Ω and T denote the peak angular

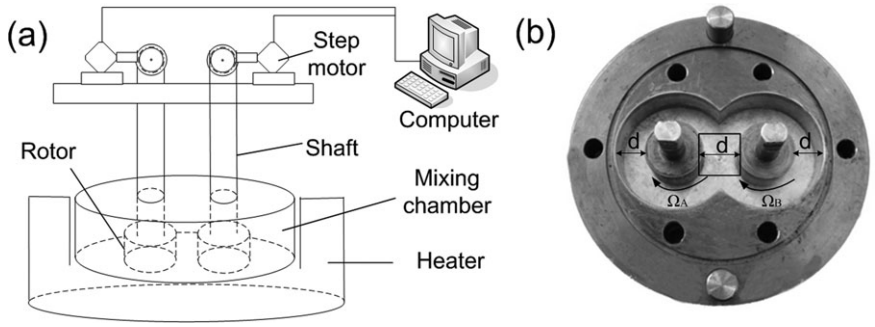

Figure 2. (a) Schematic of a batch chaotic mixer, (b) Cross-sectional view of the mixer with rotors, d is the mixing gap size, and Ω_A and Ω_B are angular speeds of rotors A and B, respectively. The square between the two rotors is the sampling zone.

speed and the time period, and are chosen to be 11 rad/s and 4.7 s for all waveforms, respectively. The angular displacement of each rotor per period, θ, can be obtained using eq. (3).

$$\theta = \int_0^T \Omega_A(t)dt = \int_0^T \Omega_B(t)dt \tag{3}$$

A value of $\theta = 1440°$ was recommended and chosen in this work, because it could produce widespread mixing in a mixing chamber.[28,34] Mixing time, t, is defined as $t = nT$, where n is the number of periods.

For the sine waveform, Ω_A and Ω_B were performed with a phase lag of 90° [Figure 3(a)]. For the square waveform, rotors A and B rotated alternately with a constant angular speed every half of T, respectively. We denote the motion which occurs due to action of the rotor A for an amount of time $T/2$ as "L" and the corresponding flow of rotor B rotation as "R." The square waveform could be described by a time-periodic sequence, i.e., "LRLRLRLRLR⋯" [Figure 3(b)].

Franjione et al.[30] proposed RP to destruct the symmetry of periodic flow and generate a self-similar pattern of "L" and "R." As an example, Figure 4 shows a protocol consisting of 32 elements. Denote the pair "LR" by "o" and "RL" by "p"; the sequence of "o" and "p" was identical to the sequence of "L" and "R." Furthermore, let "op" = "τ" and "po" = "β." It could be seen that the sequence was identical to the original. This indicated the existence of a fractal structure of mixing protocol itself.[30] RP as a recursive pattern could be expressed as "LRRLRLLRRLLRLRRL⋯", as shown in Figure 3(c).

RRS proposed by Fan and Liu[33] was a special random sequence, where no more than three repeating motions, like "LLL" or "RRR," existed. In this work, a series of restricted random numbers was created based on the random function in C language. Figure 3(d) shows an example of the RRS sequence, like "LLRLRLRRLRLRRLLR⋯."

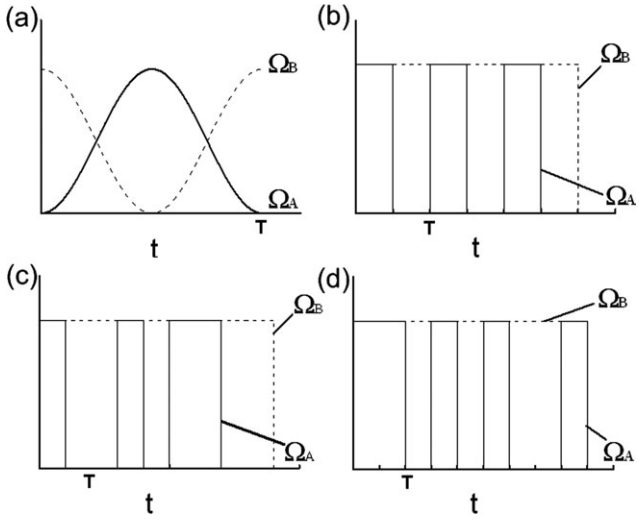

Figure 3. Different waveforms. (a) Sine, (b) square, (c) RP, (d) RRS. Solid line represents Ω_A and dotted line represents Ω_B.

Mixing Experiments

In the chaotic mixer, PP pellets were added into the narrowest zones between the rotors [Figure 2(b)] to form a block of 0.0127 m × 0.0354 m × 0.0178 m. The rest of the mixing chamber was filled with PA6 pellets. The polymer components were kept segregated until mixing began. The polymers were allowed to melt at 245°C. The rotors were delivered following different waveforms. After specified time, i.e., 8, 16, 32, 64, and 128 periods, stop the rotors and take out the sample with the square area of 0.0127 m × 0.0127 m from the gap between the two rotors [as shown in Figure 2(b)] The sample was ruptured to small fragments after quenched in liquid nitrogen to freeze-in their morphologies. The latter were characterized by scanning electron microscopy (SEM). Each experiment was repeated three times.

In the Brabender torque rheometer, the dried and premixed PP and PA6 pellets were charged into the mixing chamber, and were mixed at 50 rpm and 245°C for specified times. Samples were taken from the mixing chamber and then quenched in liquid nitrogen for further characterization. Also each experiment was repeated three times.

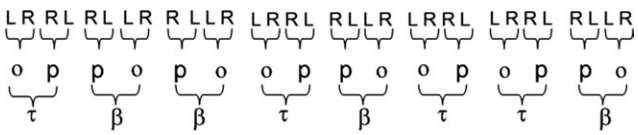

Figure 4. Illustration of the self-similarity behavior in RP.

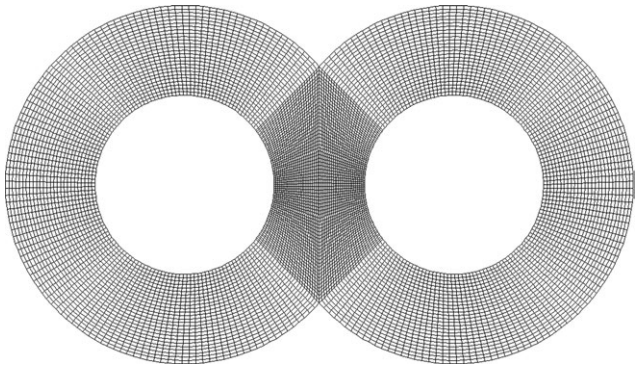

Figure 5. 2D grids of the chaotic mixer.

Scanning Electron Microscopy Characterization

SEM (ZEISS ULTRA55, Hamburg, Germany) was used to characterize the blend morphologies. Before the SEM observations, samples were fractured in liquid nitrogen and immersed in boiled xylene at 130°C refluxing for 1 h in order to etch PP domains. They were dried for 2 h in a vacuum oven at 110°C and then gold sputtered. The voltage for the SEM was 5.0 kV.

The volume mean diameters (D_v) of PP droplets were measured from several SEM images with ImageJ, an image analysis software. More than 2,700 PP droplets were used to determine the droplet size distribution for one operating condition, which can guarantee the data accuracy and reliability.

Numerical Method

Several numerical methods have been used to investigate mixing in chaotic flows including the finite element method,[35] the finite volume method,[36] the spectral element method,[37] and a mapping method.[38] The finite volume CFD package, FLUENT 6.3 (ANSYS Inc., Canonsburg, PA), was used to solve Navier–Stokes equations. The boundary conditions of the rotor motion were implemented using a user-defined function (UDF). The fine structured meshes of 9880, as shown in Figure 5, were used to reduce discretization errors in numerical simulation, along with double precision calculations to avoid round-off error.

For Lagrangian tracking, each particle was advanced in time along with the flow. For integrating fluid particle motion, velocity vectors were interpolated to particle positions using fourth-order Runge–Kutta algorithms to minimize time integration errors. Sub-iterations for the particle tracking were performed within each time step. The convergence criteria for residuals were set to 1 $e{-}5$ for variables in the simulations.

RESULTS AND DISCUSSION

Flow Number Distributions and Poincare Maps

The velocity fields in this chaotic mixer for different mixing waveforms were obtained with the CFD method. Based on these, flow number can be calculated,[39] which is defined as,

$$\chi = \frac{\gamma}{\gamma + \omega}$$

Here, γ is the magnitude of the rate of deformation tensor and ω is the magnitude of the vorticity tensor. Where, $\chi = 1.0$ signifies pure elongational flow, $\chi = 0.5$ simple shear flow, and $\chi = 0.0$ pure rotational flow.

Figure 6 shows the instantaneous distribution of the flow number with different mixing waveforms (square, sine, RP, and RRS) during one mixing period (Figure 3). The flow number distributions near the stationary rotor are quite inhomogeneous. Regions close to the walls of the mixer have a pronounced shear characteristic. The highest mixing index (about 0.95) flow appears in the middle of chamber. This corresponds to the areas of the high elongational flow and good dispersive mixing. Rotational zones are also clearly present close to the regions of the highest mixing index. These rotational zones represent a "dead" region, also called island, where the material is not deformed, but merely rotates with little exchange with the rest of the flow domain.[40]

Clearly, distinct features can be identified for the continuous (sine) and discontinuous (square, RP, and RRS) waveforms. For the sine waveform, there is a larger region of elongational flow and a more serious rotational flow region around the stationary rotor when the speeds of the rotors A and B reached their respective peak values. However, the rotational zones (weak elongational flow zones) occur during the whole period for discontinuous waveforms, because one stationary rotor always exists. The overall average flow number in the mixer during one period shows that the value for sine waveform (0.625) is larger than that for square waveform (0.603).

As for the two periodic waveforms (sine and square), the behaviors of the instantaneous distribution of flow number repeat in one period. For RP and RRS waveforms, they present the similar distribution of flow number as square waveform in one period. However, they follow the non-periodic waveform.

The velocity field solutions serve as a starting point for further characterization of the chaotic dynamics using Lagrangian tracking techniques. Poincare maps were generated by placing 600 uniformly spaced tracer particles along the vertical centerline of the mixer initially and recording the positions of these particles each period. Poincare maps, presented in Figure 7, revealed obvious islands for sine waveforms, which disappeared for other waveforms. Earlier studies also gave the same results.[13,17] The RP and RRS square waveforms provided better distributive mixing than square waveform.

Morphological Transitions

The morphologies of polymer blends for five waveforms of rotor motion were investigated with the SEM images at various mixing times in terms of the number of chaotic mixing periods.

For square waveform, the dispersed phase (PP) undergoes lamellar structure, interpenetrating network structure and droplets. Both PA6 and PP phases, which has been etched off, present lamellar structure at eight mixing periods (denoted as $8T$) as shown in Figure 8(a). The thickness of PP lamella between the two neighboring PA6 lamellas was about 10 μm. Holes (droplets of PP phase) on PA6 lamellas were found and began to emerge along the stretching direction, as shown in Figure 8(b). Hole development resulted in the formation of interconnections between adjacent PA6 lamellas and the

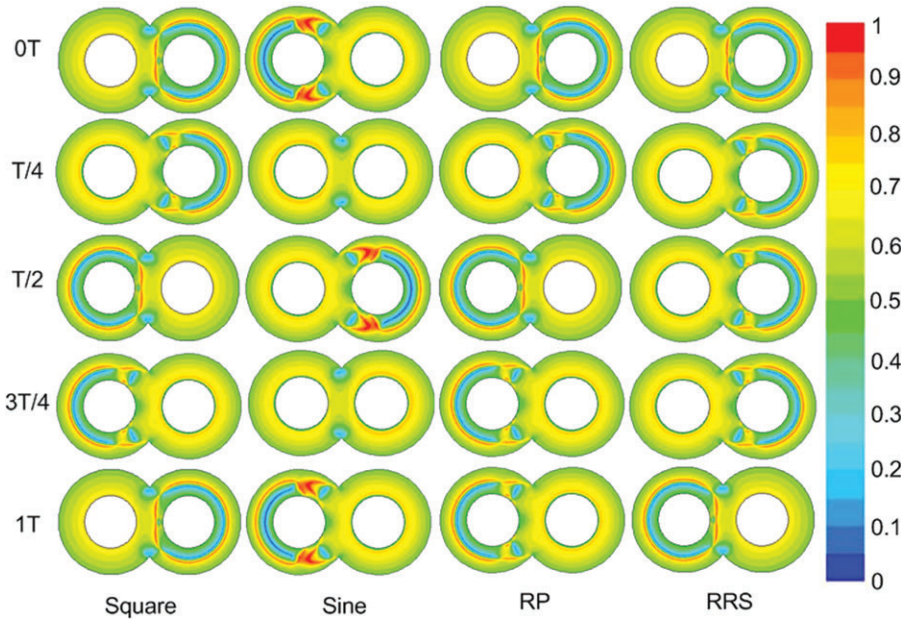

Figure 6. Instantaneous distribution of flow number with different mixing waveforms (square, sine, RP, and RRS) during one mixing period. [Color figure can be viewed in the online issue, which is available at wileyonlinelibrary.com.]

abrupt conversion of the multilayer morphology to a blend with single-phase continuity in the PA6 component, which could be examined in Figure 8(c). The formation of the interpenetrating structure was illustrated in detail for polystyrene/low-density polyethylene (PS/LDPE) blend in an eccentric cylinder chaotic mixer by Kwon and Zumbrunnen.[24]

With further mixing, the morphology tended to form sea-island structure and the refinement of droplets played a major role. The small droplets were prone to coalesce because of low interfacial tension,[41,42] while large droplets tended to breakup due to continuous stretch. Droplets exhibited narrow size distribution at mixing time of 32*T*, presented in Figure 8(d), while some large PP droplets also can be seen at mixing time of 64*T* shown in Figure 8(e). At mixing time of 128*T*, PP droplets with steady size were distributed uniformly in PA6 phase as shown in Figure 8(f). A quasi-equilibrium state is finally reached from the balance of interfacial and viscous forces and from the competition between breakup and coalescence.[28]

For the sine waveform, PP phase turns to fibril from lamella, and ultimately to droplet. In a short mixing time, the majority of PP phases exhibit lamellar structure as shown in Figure 9(a), whose thickness is almost same to that of square waveform. As

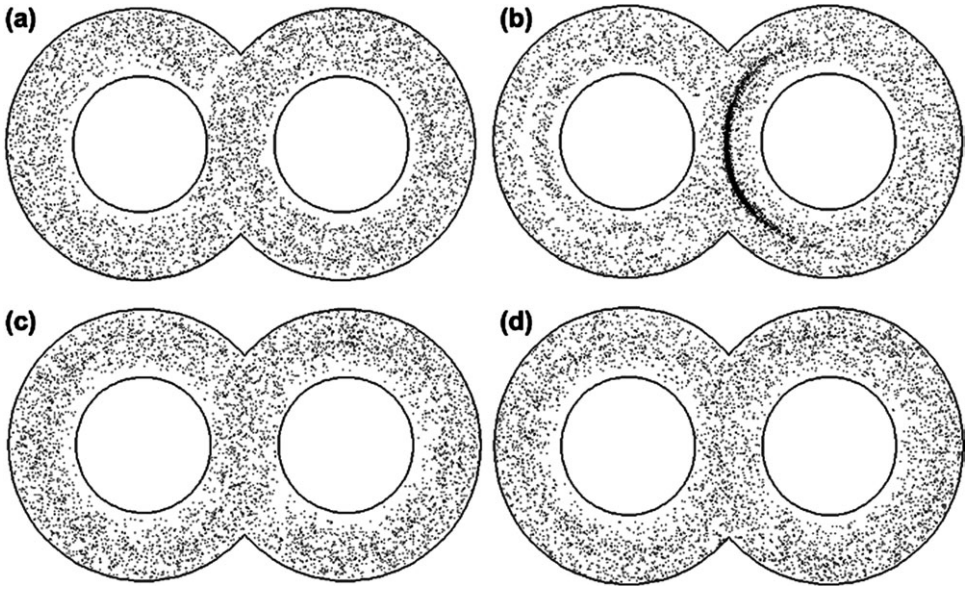

Figure 7. Poincare maps for different waveforms: (a) square; (b) sine; (c) RP; (d) RRS.

Applied Polymer SCIENCE

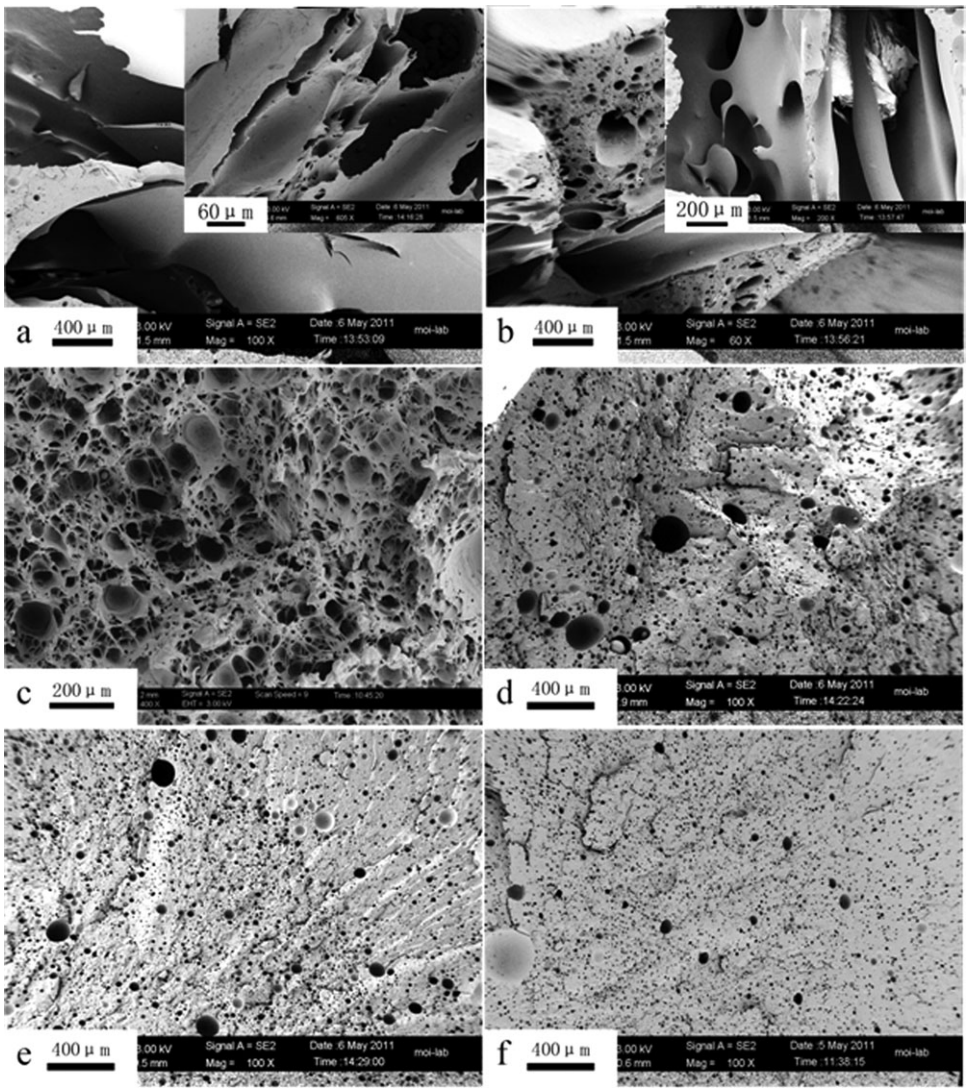

Figure 8. Morphology of PA6/PP (90/10) blends in the chaotic mixer for the square waveform at different mixing times, (a) 8*T*, lamellar structures; (b) 8*T*, fibrillar structures; (c) 16*T*; (d) 32*T*; (e) 64*T*; (f) 128*T*.

revealed in Figure 9(b), the PP fibrils are distributed in parallel along the stretching direction. The fibrillar diameter was almost consistent with the thickness of PP lamella, because the fibrils were formed from the fracture of lamellas. Both fibrillar and lamellar structures existed at mixing time of 8*T*, but the lamellar morphology took the dominant position. As shown in Figure 9(c), some lamellar structures still exist and more large droplets are observed. The fibrillar structure still could be observed at mixing time of 32*T*, presented in Figure 9(d), but with the formation of larger and non-uniform droplets. At mixing time of 64*T*, the distribution of droplet size was narrower as shown in Figure 9(e). It will be seen from Figures 8(f) and 9(f) that PP droplets for sine waveform are smaller than those for square waveform, while large droplets are less due to more uniform stretching at mixing time of 64*T*. Sine waveform performs larger elongational flow than those waveforms based on the square, presented in Figure 6.

It can be seen from Figure 3 that for square waveform in a time period *T*, rotor A is in motion for the first *T*/2, while rotor B remains stationary. In turn, rotor B turns in the second *T*/2 with rotor A remaining stationary. Therefore, a weak stretching zone always exists around the stationary rotor for half of a period (as shown in Figure 6), where fibrils may break up prematurely leading to large droplets. Therefore, the sine waveform continuously stretches fibrils and reduces the duration time of weak stretching zone. It provides more uniform stretch and produces faster morphology transition than square waveform.[29]

The morphology transition of the PP phase of the RP waveform is similar to that of the sine waveform. However, the transition is faster and no obvious lamellas and fibrils are found at the mixing time of 16*T*. In Figure 10(a), a small number of large droplets exist along with fibrils. With further mixing, the droplet size gradually decreases and its distribution becomes

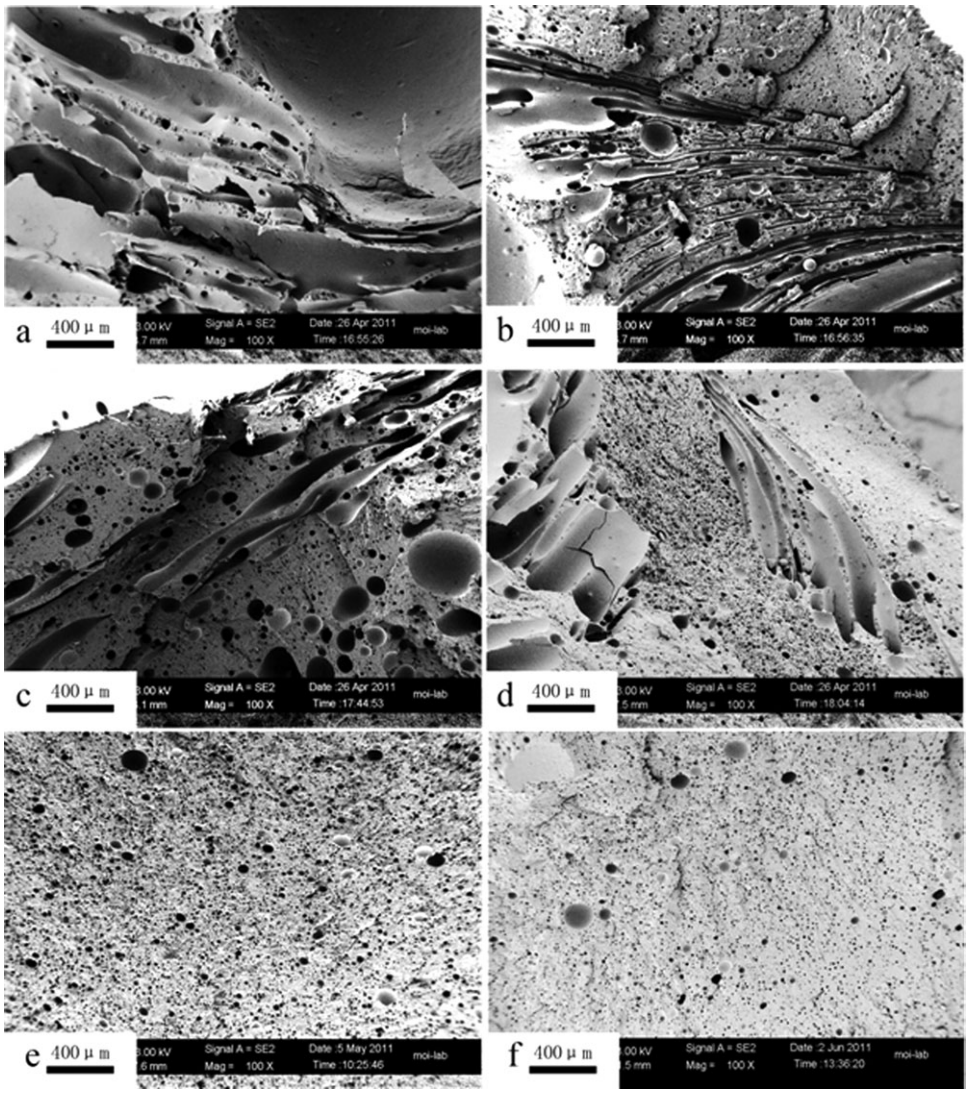

Figure 9. Morphology of PA6/PP (90/10) blends in the chaotic mixer for the sine waveform at different mixing times, (a) 8*T*, lamellar structures; (b) 8*T*, fibrillar structures; (c) 16*T*; (d) 32*T*; (e) 64*T*; (f) 128*T*.

narrower, as shown in Figure 10(b–d) at the mixing times of 16*T*, 32*T*, and 64*T*. As mentioned above, RP can eliminate islands existed in a periodic chaotic mixing flow[30] and creates chaotic mixing in the whole mixing zone. The corresponding spatial stretching distribution of the polymer blends is more uniform than that for sine waveform. Therefore, its final blend morphology shows smaller droplets with a narrow size distribution [see Figure 10(e)].

In the case of RRS mixing waveform, the PP phase is not dispersed throughout the continuous phase in a short mixing time. There are still areas with smooth surfaces which contain the pure PA6 phase, as shown in Figure 11(a). The content of the lamellar structure is very low at 16*T* [Figure 11(b)]. The droplets gradually decrease in size and their distribution becomes narrower as shown in Figure 11(c, d) at the mixing time of 32*T* and 64*T*, respectively. For the initial several periods in this case, the sequence, "LLRRLLRRLLRRLRLLRRLRRLRLRLLRLLRR…," is much like a square waveform with twofold period besides randomly appeared sequence segments with one period. It is known that mixing is poor when the oscillation of the speed of the rotors is too frequent or too slow. When the speed oscillates slowly, chaotic mixing is limited to a narrow band near the homoclinic orbit resulting in uneven distribution of the dispersed phase.[16,43] Therefore, the RRS performs poor mixing initially, resulting in poorer mixing efficiency and bigger droplet diameter than those for RP at a long mixing time, as shown in Figures 10(e) and 11(e). Due to the relatively high randomness of RRS itself, some sequences may be able to lead to good mixing performance, like RP which is a special case of RRS. However, others may cause bad mixing efficiency, like "LLRLLRLLRLLR" or "RRLRRLRRLRRL" which provides uneven distribution of stretching for the two zones surrounding the rotors.

For mixing in the Brabender torque rheometer, both the dispersed and continuous phases are broken up by strong shear of roller blades to form a sea-island structure. Strong shear is helpful for forming smaller droplets but with a wider size distribution.

Applied Polymer SCIENCE

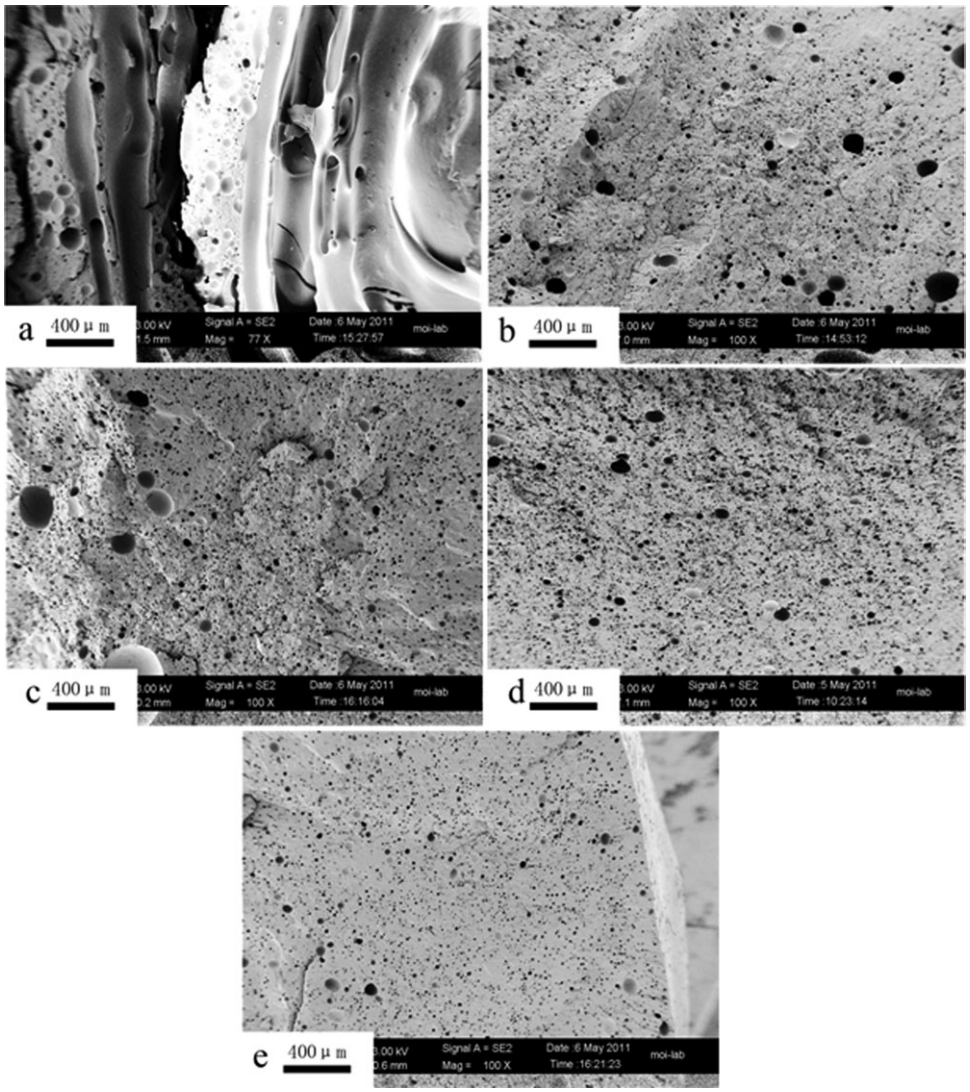

Figure 10. Morphology of PA6/PP (90/10) blends in the chaotic mixer for RP at different mixing times, (a) 8*T*; (b) 16*T*; (c) 32*T*; (d) 64*T*; (e) 128*T*.

The initial blend system is mixed non-uniformly with much unmixed areas of the pure PA6 due to low shear strain, as shown in Figure 12(a). At the mixing time of 32*T*, there are still unmixed areas of the pure PA6 and very large droplets, shown in Figure 12(b). Very small droplets coexist with very large ones at long mixing times [Figure 12(c–e)]. Morphologies, like lamellar and fibrillar structures, cannot be found from SEM images, because their transition process is too fast to be captured.[4]

Compared with the periodic waveforms (square and sine), the non-periodic sequences (RP and RRS) undergo the similar pathway of the morphology development, from lamellas to fibrils and to droplets. Based on the large number of SEM images, the morphology transition speed of the PP phase follows the order: RP > sine > square > RRS.

Droplet Size

The influences of the waveform of the rotor motion on the droplet size are investigated. Figure 13 shows the evolution of the volume mean diameter with various stages of mixing which reveals the relative importance of the breakup of fibrils and the coalescence of droplets.

As a general trend, during the early stage of mixing, the majority of fibrils break up into droplets, and coalescence takes place at long mixing times causing coarsening of the droplet population. The droplet morphology transitions for RP and traditional mixing in the Brabender torque rheometer are faster than those for the other waveforms.

The curve for the traditional mixing in the Brabender torque rheometer is relatively flat. The polymer have undergone strong shear to break up into small droplets in a very short time. The droplet size decreases with increasing shear strain until a certain value below which droplets are prone to coalescence. After a mixing time of 48*T* in the Brabender torque rheometer, an equilibrium between coalescence and breakup is reached and droplets remain unchanged in size, as shown in Figure 13.

The largest droplet size reaches 22 μm at 16*T* for RRS due to the initial protocol as "LLRRLLRRLLRRLRLLRRLRRLRLRLLRLLRR," where more sequence segments as "LL" and "RR" exist and provide

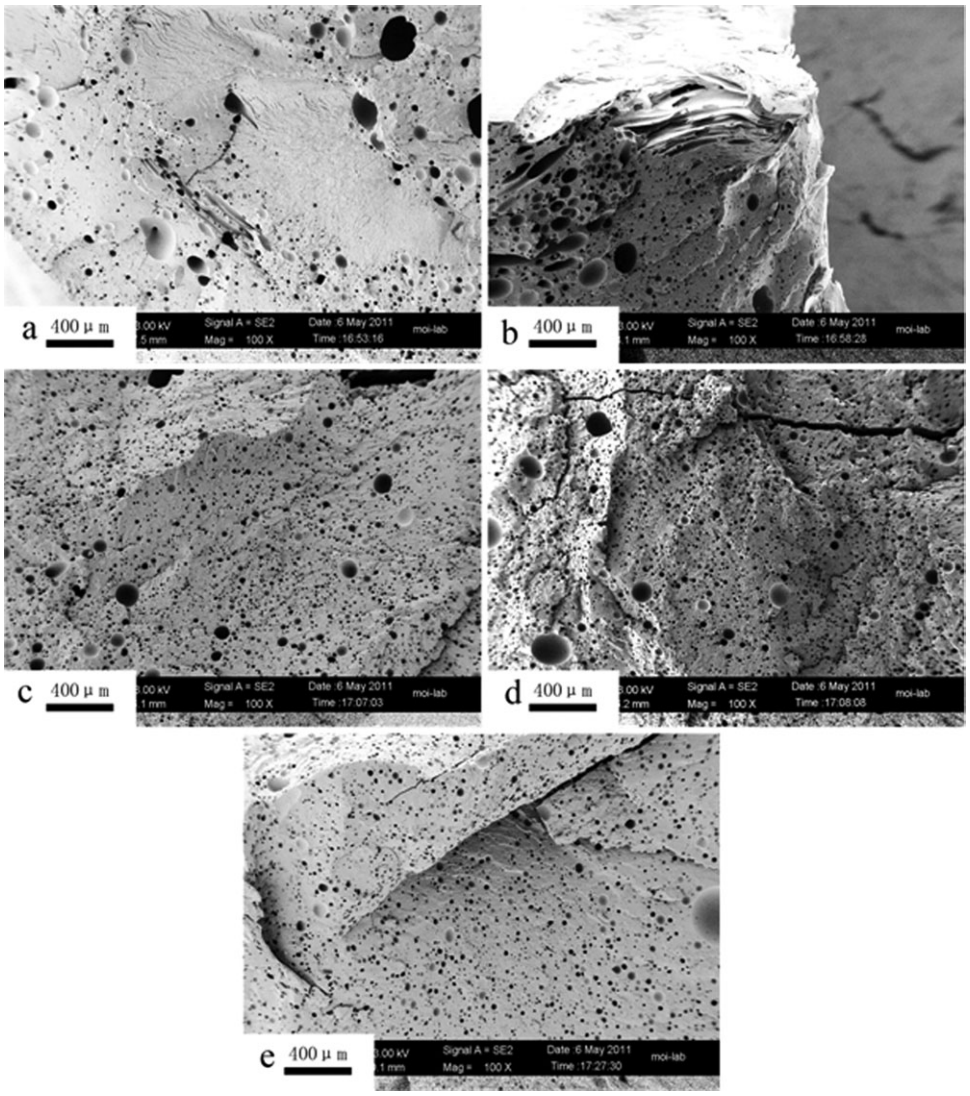

Figure 11. Morphology of PA6/PP (90/10) blends in the chaotic mixer for RRS at different mixing times, (a) 8*T*; (b) 16*T*; (c) 32*T*; (d) 64*T*; (e) 128*T*.

the weak stretching zone with a longer time, resulting in larger droplets. During 16*T*–64*T*, the droplet size decreases rapidly but is still larger than the others. A similar trend is found for the square waveform.

From Figure 13, in the case of the sine waveform the droplet size decreases until coalescence starts to be obvious at 64*T*, which is slower than that for RP. During the very early period, the droplet size for RP decreases sharply to 10.7 μm at 32*T*. It can be attributed to the non-periodic chaotic mixing which help stretch fibrils intensively and break them up to small droplets with a narrow distribution. RP shows a smaller droplet size than square waveform and RRS.

In addition, for all kinds of waveforms the droplet size after 64*T* starts to level off due to the balance of competition between breakup and coalescence, and the equilibrium sizes fall in a narrow range from 12 to 13.5 μm under the almost same processing parameters (shear rate and total strain) and material parameters such as viscosity ratio, dynamic interfacial tension, and concentration of the dispersed phase.

Droplet Size Distribution

The sine and RP waveforms are chosen to compare the droplet size distribution due to their good mixing performance mentioned in Figure 13 and Figures 8–12. Table I presents a breakdown of droplets in number% above 20 μm, below 10 μm, and between 10 and 20 μm for sine and RP waveforms at different mixing times.

The concentration of large droplets (above 20 μm) decreases first. As long as the effect of coalescence plays an important role, the concentration of the large droplets increases and is stable. For the sine waveform, the lowest content of large droplets appears at 64*T*, and the droplet size is also the smallest. For the RP, it appears at 32*T*, earlier than the sine waveform, indicating that the development of morphology for RP is faster. The content of small droplets (below 10 μm) for RP is always higher than that for the sine waveform. When the droplet size reaches a quasi-stable state, the content of large droplets is slightly lower for the RP.

The different behavior in droplets size between the sine and RP waveforms is directly related to islands in a periodic chaotic

Applied Polymer SCIENCE

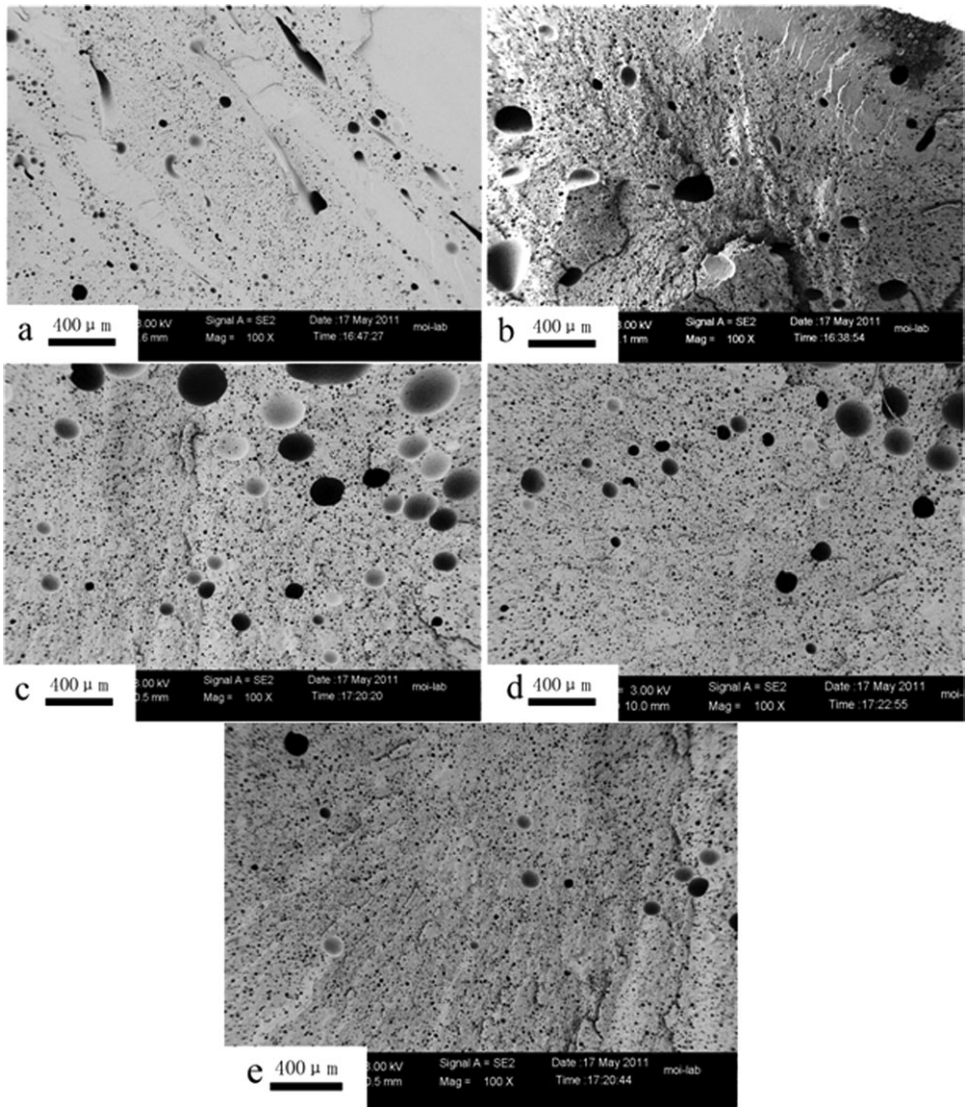

Figure 12. Morphology of PA6/PP (90/10) blends in the Brabender torque rheometer for steady waveform at different mixing times, (a) 16*T*; (b) 32*T*; (c) 48*T*; (d) 64*T*; (e) 128*T*.

mixing flow. Poincare maps, presented in Figure 7, reveal obvious islands which exist between the rotors and the wall of mixing chamber for the sine waveform and which do not exist for the RP waveform. Mixing inside the islands is poor, resulting in coalescence of small droplets to large ones. The RP can effectively eliminate islands by destructing the symmetry of periodic mixing and creating chaotic flow in the whole mixing zone. Therefore, the final blend morphology shows smaller droplets with a narrow size distribution.

Figure 14 shows the droplet size distribution of the droplet size for different waveforms at a mixing time of 64*T*. The RP waveform yields the narrowest droplet size distribution. Those of the sine waveform and traditional mixing flow in the Brabender torque rheometer are similar to that of the RP. The RRS waveform generates the widest droplet size distribution a large volume fraction of large droplets.

From Figures 13 and 14, D_v is controlled by a few "large droplet events" as large droplets play an important role in its value. A large number of data are used to determine the droplet size and its distribution. The overall shapes of the droplet size distribution are similar for different waveforms, indicating that the contribution of large droplets to D_v is almost the same for these cases.

This work has focused on non-reactive polymer blends and is currently being extended to reactive ones using different types of functionalized polymers.[44–48]

CONCLUSIONS

The flow number distributions for different waveforms of the rotor motion show that the sine waveform performs stronger elongational flow than those based on the square. Poincare maps show that the square type waveforms provide better distributive mixing.

Experimental results show that the morphologies of the dispersed phase for all kinds of waveforms of the rotor motion follow the same development pathway: from lamellas to fibrils and

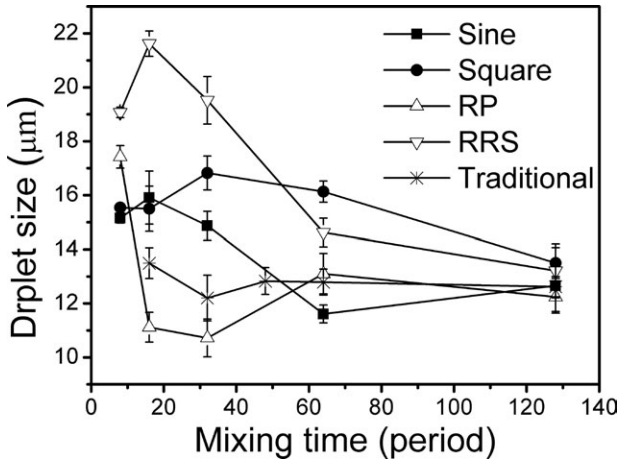

Figure 13. Droplet size of the PP domains for different waveforms (sine, square, RP, RRS, and Brabender torque rheometer) at different mixing times.

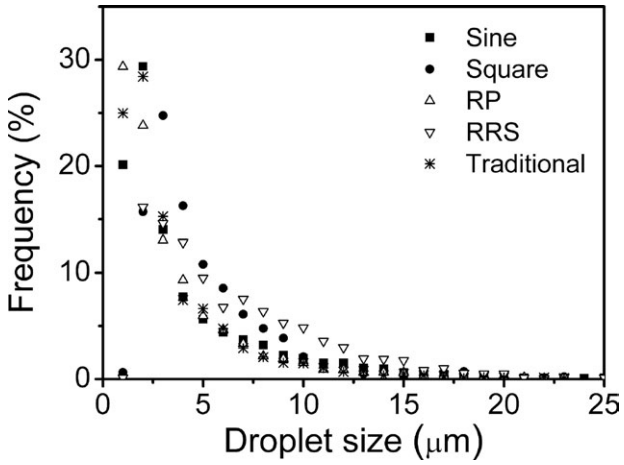

Figure 14. Frequency distribution of droplet size for different waveforms (sine, square, RP, RRS, and Brabender torque rheometer) at a mixing time of 64*T*.

then to droplets. The size of droplets obtained after a long mixing time or a large total strain tends to fall in a small range, indicating that the equilibrium diameters of droplets are independent of the type of the waveform.

RP creates chaotic mixing with a non-periodic waveform of the rotor motion and yields the best performance in terms of the morphology development of the PP and PA6 blends. The dispersed phase is rapidly stretched to fibrils and the latter are transformed to smaller droplets with a narrow distribution. This high performance is attributed to the uniform spatial stretching distribution and the absence of islands in the mixing region.

However, the mixing performance of a non-periodic waveform is not always as good as that of the RP waveform. The sequences of RRS may provide poor mixing performance due to their stochastic generation mechanism. Therefore, the waveform sequence is very important for a non-periodic flow. From the engineering viewpoint, the RP waveform has a higher potential in industry. Comparison of the droplet size and its distribution between the RP and sine waveforms indicates that spatial unmixed regions (islands) have larger negative effects than temporal unmixed ones (weak stretching zone).

Table I. Droplets in Number % Above 20 μm, Below 10 μm, and Between 10 and 20 μm for Sine and RP Waveforms at Different Mixing Times

		Number %		
Waveform	Mixing time	$0 < D_v < 10$ μm	$10 < D_v < 20$ μm	$D_v > 20$ μm
Sine	8*T*	90.22	8.92	0.50
	16*T*	92.38	7.13	0.24
	32*T*	94.87	4.52	0.18
	64*T*	93.04	6.22	0.06
	128*T*	88.82	10.93	0.29
RP	8*T*	95.06	4.23	0.71
	16*T*	95.37	4.47	0.16
	32*T*	96.68	3.27	0.05
	64*T*	95.04	4.73	0.23
	128*T*	92.51	7.22	0.27

ACKNOWLEDGMENTS

This work was supported by Zhejiang Provincial Natural Science Foundation of China (Y4090319), Natural Science Foundation of China (NSFC) (50503020), and State Key Laboratory of Chemical Engineering (SKL-ChE-11D01).

REFERENCES

1. Lindt, J. T.; Ghosh, A. K. *Polym. Eng. Sci.* **1992,** *32*, 1802.
2. Scott, C. E.; Macosko, C. W. *Polymer* **1995,** *36*, 461.
3. Scott, C. E.; Macosko, C. W. *Polym. Bull.* **1991,** *26*, 341.
4. Lyngaae-Jorgensen J. *J. Macromol. Sci. Part B: Phys.* **1996,** *35*, 357.
5. Sundararaj, U.; Macosko, C. W.; Rolando, R. J.; Chan, H. T. *Polym. Eng. Sci.* **1992,** *32*, 1814.
6. Ghosh, A. K.; Ranganathan, S.; Lindt, J. T.; Lorex, S. *Proc. SPE ANTEC* **1991,** *37*, 232.
7. Jana, S. C.; Sau, M. *Polymer* **2004,** *45*, 1665.
8. Erwin, L. *Polym. Eng. Sci.* **1978,** *18*, 1044.
9. Erwin, L. *Polym. Eng. Sci.* **1978,** *18*, 572.
10. Pinheiro, L. A.; Hu, G. H.; Pessan, L. A.; Canevaro, S. V. *Polym. Eng. Sci.* **2008,** *48*, 806.
11. Kim, S. J.; Kwon, T. H. *Adv. Polym. Technol.* **1996,** *15*, 41.
12. Jones, S. W.; Metcalfe, G.; Ottino, J. M. *J. Fluid Mech.* **1989,** *209*, 335.
13. Jana, S. C.; Tjiahjadi, M.; Ottino, J. M. *AIChE J.* **1994,** *40*, 1769.

14. Aref H. *J. Fluid Mech.* **1984,** *143*, 1.
15. Ottino, J. M. The Kinematics of Mixing: Stretching, Chaos, and Transport; Cambridge University Press: New York, **1989.**
16. Jana, S. C.; Metcalfe, G.; Ottino, J. M. *J. Fluid Mech.* **1994,** *269*, 199.
17. Leong, C. W.; Ottino, J. M. *J. Fluid Mech.* **1989,** *209*, 463.
18. Niederkorn, T. C.; Ottino, J. M. *J. Fluid Mech.* **1993,** *256*, 243.
19. Swanson, P. D.; Ottino, J. M. *J. Fluid Mech.* **1990,** *213*, 227.
20. Kusch, H. A.; Ottino, J. M. *J. Fluid Mech.* **1992,** *236*, 319.
21. Ottino, J. M.; Ranz, W. E.; Macosko, C. W. *Chem. Eng. Sci.* **1979,** *34*, 877.
22. Miles, K. C.; Nagarajan, B.; Zumbrunnen, D. A. *J. Fluids Eng.* **1995,** *117*, 582.
23. Zumbrunnen, D. A.; Miles, K. C.; Liu, Y. H. *Composites A* **1996,** *27*, 37.
24. Kwon, O.; Zumbrunnen, D. A. *J. Appl. Polym. Sci.* **2001,** *82*, 1569.
25. Zumbrunnen, D. A.; Subrahmanian, R. *Adv. Polym. Technol.* **2006,** *25*, 152.
26. Zumbrunnen, D. A.; Inamdar, S. *Chem. Eng. Sci.* **2001,** *56*, 3893.
27. Zumbrunnen, D. A. *J. Text. Inst.* **2000,** *91*, 92.
28. Sau, M.; Jana, S. C. *Polym. Eng. Sci.* **2004,** *44*, 407.
29. Sau, M.; Jana, S. C. *AIChE J.* **2004,** *50*, 2346.
30. Franjione, J. G.; Leong, C. W.; Ottino, J. M. *Phys. Fluids* **1989,** *11*, 1772.
31. Liu, M.; Muzzio, F. J.; Peskin, R. L. *Chaos, Solut. Fractal* **1994,** *4*, 869.
32. Liu, Y. H.; Zumbrunnen, D. A. *J. Mater. Sci.* **1999,** *34*, 1921.
33. Fan, Y. R.; Lu, Z. M. *J. Chem. Ind. Eng. (China)* **2002,** *53*, 659.
34. Chien, W. L.; Rising, H.; Ottino, J. M. *J. Fluid Mech.* **1986,** *170*, 355.
35. Fountain, G. O.; Khakhar, D. V.; Mezic, I.; Ottino, J. M. *J. Fluid Mech.* **2000,** *417*, 265.
36. Wang, J. J.; Feng, L. F.; Ottino, J. M.; Lueptow, R. *Ind. Eng. Chem. Res.* **2009,** *48*, 2436.
37. Bar-Yoseph, P. Z.; Fisher, D.; Gottlieb, O. *Comput. Mech.* **1996,** *18*, 302.
38. Galaktionov, O. S.; Anderson, P. D.; Kruijt, P. G. M.; Peters, G. W. M.; Meijer, H. E. H. *Comput. Fluids* **2001,** *30*, 271.
39. Yao, C. H.; Manas-Zloczower I. *Int. Polym. Process* **1997,** *7*, 92.
40. Jongen, T. *AIChE J.* **2000,** *46*, 2104.
41. Chesters, A. *Chem. Eng. Res. Des. A* **1991,** *69*, 259.
42. Jenssen, J. M. H.; Meijer, H. E. H. *Polym. Eng. Sci.* **1995,** *35*, 1766.
43. Kaper, T. J.; Wiggins, S. *J. Fluid Mech.* **1993,** *253*, 211.
44. Hu, G. H.; Scaffaro, R.; La Mantia, F. *J. Macromol. Sci. A* **1998,** *35*, 457.
45. Hu, G. H.; Cartier, H. *J. Appl. Polym. Sci.* **1999,** *71*, 125.
46. Hu, G. H.; Li, H.; Feng, L. F.; Pessan, L. A. *J. Appl. Polym. Sci.* **2003,** *88*, 1799.
47. Cartier, H.; Hu, G. H. *Polym. Eng. Sci.* **1998,** *38*, 177.
48. Hu, G. H.; Li, H.; Feng, L. F. *Macromolecules* **2002,** *35*, 8247.